THE JOURNAL OF PHYSICAL CHEMISTRY C

Article

Cite This: J. Phys. Chem. C 2018, 122, 22688−22698

pubs.acs.org/JPCC

Graphyne Nanotubes: Materials with Ultralow Phonon Mean Free Path and Strong Optical Phonon Scattering for Thermoelectric Applications

Amin Reihani,[†,#] Alireza Soleimani,[‡,#] Sajad Kargar,[§] Veera Sundararaghavan,[∥] and Ali Ramazani*[,∥,⊥]

[†]Department of Mechanical Engineering, University of Michigan, Hayward Street, 2350 Ann Arbor, United States

[‡]Department of Physics, Amirkabir University of Technology, P.O. Box 15875-4413, Tehran 64540, Iran

[§]Center of Excellence in Energy Conversion (CEEC), School of Mechanical Engineering, Sharif University of Technology, Azadi Avenue, P.O. Box 11365-9567, Tehran 11155, Iran

[∥]Department of Aerospace Engineering, University of Michigan, Beal Avenue, 1320 Ann Arbor, United States

[⊥]Department of Mechanical Engineering, Massachusetts Institute of Technology, 77 Massachusetts Avenue, Cambridge 02139, United States

Supporting Information

ABSTRACT: Thermal conductivity and phonon transport properties of graphyne nanotubes (GNTs) and conventional carbon nanotubes (CNTs) are studied using nonequilibrium molecular dynamics simulations. The effect of nanotube length on the thermal conductivity and phonon transport transition from a ballistic to a diffusive regime is investigated. It is found that the thermal conductivity is significantly higher for CNTs in comparison to that of GNTs across the entire ballistic−diffusive transport range. Among GNTs, β- and γ-GNTs demonstrated the lowest and highest thermal conductivities, respectively. In addition, ultralow ballistic to diffusive transition length (4.5−7.6 nm) was observed in GNTs, which was significantly lower compared to CNTs. This behavior is due to the extremely low phonon mean free path (MFP), which is primarily due to a higher phonon scattering rate in a graphyne lattice. In the diffusive regime, the thermal conductivity does not converge at lengths up to 200 nm for both GNTs and CNTs; however, the rate of increase in thermal conductivity of GNTs as a function of nanotube length was considerably lower compared to CNTs. Statistical analysis of umklapp phonon−phonon scattering events indicated that high-energy optical phonon modes which are generated by acetylene bonds in GNTs play a major role in scattering and limiting the MFP of heat carriers, leading to significantly shorter ballistic to diffusive transition length in GNTs. Because of a low rate of electron−phonon scattering, the electron MFP in GNTs was estimated to be extremely large and in a microscale range at room temperature. This, in conjunction with ultralow phonon MFP, provides a pathway toward high thermoelectric figure of merit in long GNTs.

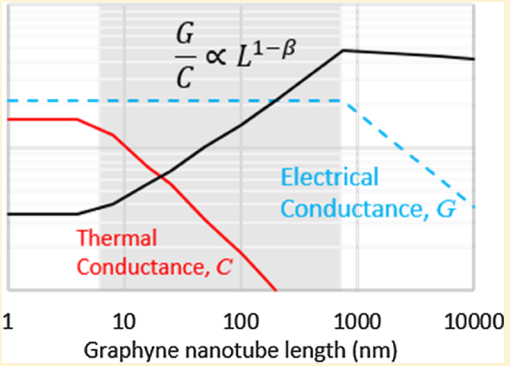

1. INTRODUCTION

Thermal properties of materials at the nanoscale have attracted extensive attention of the scientific community in recent years.[1] Recent thermal management strategies in nanofabricated devices necessitate the development of more effective heat-conducting materials.[2] Different carbon allotropes such as graphene, diamond, and carbon nanotubes (CNTs) are considered as materials with extremely large thermal conductivity as a result of their atomic structures.[3−5] Numerous experimental studies have been carried out to measure the thermal conductivity of theses allotropes. For example, Kim et al. measured the thermal conductivity of a single-walled CNT (SWNT) using a microfabricated suspended device. They indicated that the phonon mean free path (MFP) is 500 nm at room temperature and the thermal conductivity is more than 3000 W m^{-1} K^{-1}.[6] Guthy et al. prepared SWNT−PMMA nanocomposites using random SWNT orientation with nanotube loadings as high as 9 vol %. They measured a 240% increase in the thermal conductivity with nanotube loading of 6 vol %. They also showed that increasing nanotube loading does not affect the thermal conductivity because of poor nanotube dispersion at high concentration.[7] Using the four-pad 3ω method, Wang et al. reported that the thermal conductivity of individual SWNTs increases along with length over the range of 0.5−7 μm.[8]

Received: June 20, 2018
Revised: September 2, 2018
Published: September 3, 2018

DOI: 10.1021/acs.jpcc.8b05898
J. Phys. Chem. C 2018, 122, 22688−22698

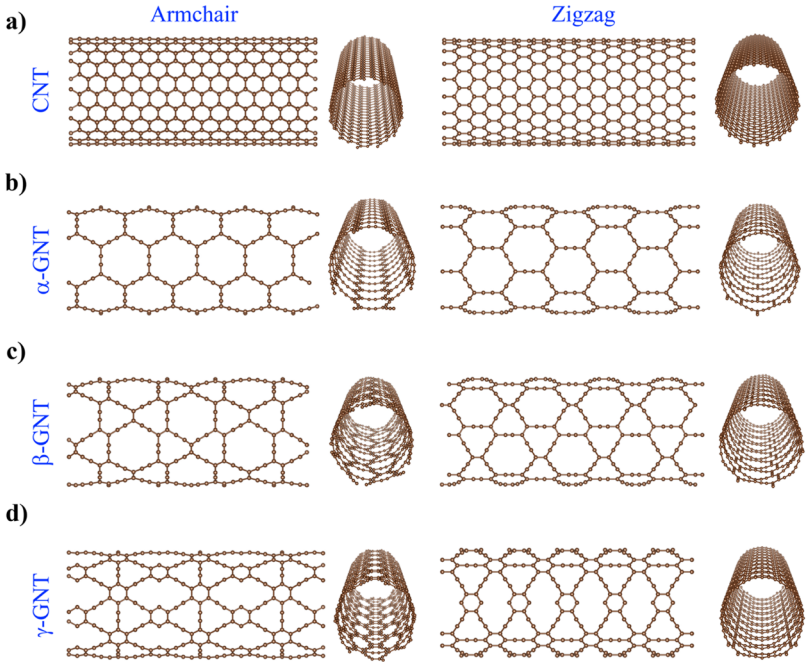

Figure 1. Schematic representation of graphene and graphyne lattice structure, as well as armchair and zigzag nanotubes for (a) CNT, (b) α-GNT, (c) β-GNT, and (d) γ-GNT.

As thermal measurement of nanostructures is challenging because of limitations of experimental techniques at nanoscales, atomistic techniques such as molecular dynamics (MD) simulations are used as an alternative approach to explore the thermal properties of nanostructured materials. On the basis of classical MD techniques, we employed an atomistic model using a force field to describe interactions between atoms, which follows classical Newtonian dynamics.[9] Numerous studies have employed MD simulations to calculate the thermal conductivity of nanomaterials. Generally, four different MD methods can be used to calculate the thermal conductivity: equilibrium MD which is based on the Green−Kubo formula, nonequilibrium MD (NEMD) and reverse nonequilibrium MD (RNEMD) which are based on the Fourier's law of heat conduction, and homogenous nonequilibrium MD in which an external field is applied to the system.[10−12]

Salaway and Zhigilei investigated the thermal conductivity of (10, 10) CNTs in a wide range of lengths varying from 47 to 630 nm using the NEMD method. They demonstrated that for CNTs shorter than 200 nm, the length dependence is much stronger than that of longer CNTs, indicating a transition from a ballistic to a diffusive−ballistic heat transport regime.[13] Alaghemandi et al. performed RNEMD simulations to study the effect of temperature, length, and chiral index on the thermal conductivity of single-walled and multi-walled CNTs in a wide temperature range varying from 200 to 1000 K. It was shown that as the temperature increases, the thermal conductivity decreases; in addition, the thermal conductivity increases with the nanotube length.[14] Lukes and Zhong employed equilibrium MD to investigate the thermal conductivity of SWNTs as a function of temperature ranging from 100 to 500 K at different nanotube lengths using both free and periodic boundary conditions. They reported that as the temperature increases, the thermal conductivity decreases.[2]

Graphyne is a class of graphene allotropes which contains sp- and sp^2-hybridized carbon atoms forming C−C and C≡C bonds resulting in various optical, electronic, and thermal properties.[15] The atomic structure of graphyne has three main symmetric types; α-, β-, γ-graphyne with 33.3, 28.6, and 20.0% carbon triple bonds, respectively. Analogous to CNT, graphyne nanotubes (GNTs) can be formed by rolling up the graphyne sheet into cylinders.[16] A number of studies have been performed to investigate the thermal properties of graphyne-based materials. Wang et al. studied the heat transport of carbon allotrope sheets employing NEMD simulations and reported that not only the acetylenic linkages significantly reduce the thermal conductivity, but they can also tune the thermal conductivity through different bonding methods. A new approach was then proposed to manipulate the thermal conductivity through the assembling of acetylenic linkages.[17] Zhang et al. carried out RNEMD simulations to predict the thermal conductivity of different graphyne and graphene sheets. It was found that in comparison with graphene, graphyne has a lower thermal conductivity because of the existence of acetylenic bonds. In addition, they reported that the structure, external strain, and temperature have an influence on the thermal conductivity of graphynes.[5] Pan et al. carried out NEMD simulations to explore the thermal conductivity of graphyne nanoribbons as a function of orientation and temperature. They reported that in comparison with zigzag orientation, the thermal conductivity of armchair orientation with identical length and width is larger. It was also indicated that regardless of the orientation, as the temperature rises from 200 to 800 K, the thermal conductivity decreases.[18] Hu et al. investigated the heat transport of perfect-phase GNTs using NEMD. The atomic structure of these materials, which consist of a weak acetylenic linkage and a strong hexagonal ring, contributes to a large vibrational mismatch, resulting in an unprecedentedly low thermal conductivity.[19]

The main purpose of this paper is to determine the role of an acetylene bond in phonon transport mechanism in GNTs and the transition from a ballistic to a diffusive transport regime. Therefore, NEMD simulations have been carried out

DOI: 10.1021/acs.jpcc.8b05898
J. Phys. Chem. C 2018, 122, 22688−22698

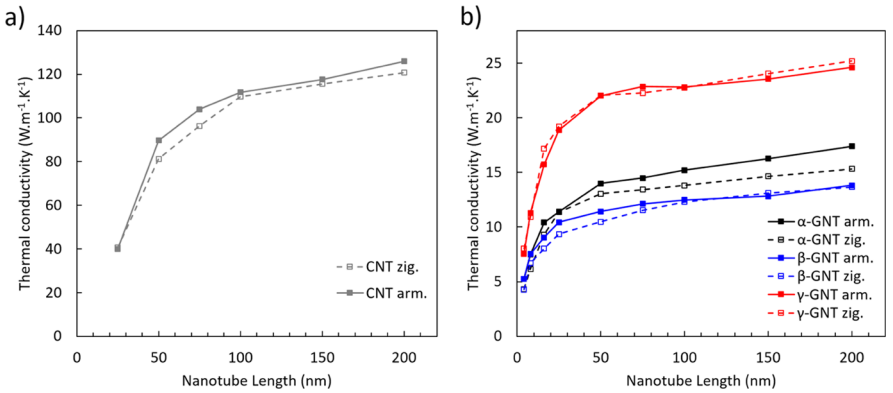

Figure 2. Thermal conductivity as a function of length at 300 K for (a) CNTs and (b) GNTs.

to determine the thermal transport parameters of α-, β-, and γ-GNTs with a wide range of nanotube lengths at room temperature. Figure 1 depicts the atomic structures of GNT and CNT in both zig-zag $(n, 0)$ and armchair (n, n) orientations used in MD simulations. The index numbers of nanotubes are (4, 4) and (7, 0) for armchair and zigzag α-GNT, respectively. Similarly, they are (4, 4) and (7, 0) for β-GNTs, (3, 3) and (5, 0) for γ-GNT, and (11, 11) and (19, 0) for CNTs, respectively.

2. COMPUTATIONAL METHODOLOGY

2.1. Thermal Properties. Simulations are carried out to investigate the phonon transport properties of single-walled CNTs and GNTs as a function of length ranging from 4 to 200 nm in various phases and orientations at room temperature. Calculations were done in the large-scale atomic/molecular massively parallel simulator software package.[20] The minimum and maximum lengths are chosen in a wide range where the transition length can be determined. Calculation of phonon interaction rates and phonon spectrum requires inclusion of both the harmonic and anharmonic interatomic force constants, which were obtained using a second-generation reactive empirical potential. A velocity-Verlet integrator was used to integrate the equations of motion.[21] Periodic boundary conditions were applied in all directions, where the first and last rings of carbon atoms at the two ends of the nanotube have been fixed in order to prevent structural instability and maintain the heat flux direction along the nanotube axis during the simulation. Furthermore, the initial structural energy minimization is performed using the conjugate gradient algorithm. In addition, a Nose−Hoover thermostat is used to equilibrate the systems in a canonical ensemble (NVT) with the time step of 1 fs for 0.5 ns.[22] To avoid any instability in calculation of the thermal conductivity, the total linear and angular momentum of the systems are set to zero. To calculate the thermal conductivity of CNTs and GNTs using NEMD simulations, a stable-temperature gradient needs to be stablished along the longitudinal direction by transferring heat flux from one region of the system (hot region) to another one (cold region). The temperatures in the hot and cold bath regions are set to be $T + \Delta T/2$ and $T - \Delta T/2$, respectively, where T is the average temperature and ΔT is the temperature difference created over the two ends of the nanostructure, which is set to $\Delta T = 50$ K for all simulations. To make sure that the system has reached a nonequilibrium steady-state condition, simulations are continued for 20 ns. After ensuring that the temperature distribution is time-independent, the heat flux, J (W m^{-2}) is calculated using eq 1, where V (m^3) is the system volume and ε_i (J) is the per atom total energy of atom i obtained by summation of kinetic and potential energy of the ith atom. S_i is the symmetric per atom stress tensor (with units of stress volume, i.e., N m) and v_i (m s^{-1}) is the velocity vector.[23]

$$J = \frac{1}{V}\left(\sum_i \varepsilon_i v_i - \sum_i S_i v_i\right) \quad (1)$$

The nanostructure thermal conductivity can be obtained according to Fourier law of heat conduction from eq 2,[24] where k_{MD} (W m^{-1} K^{-1}) represents the MD thermal conductivity, J is the heat flux, and dT/dz is the temperature gradient in the longitudinal direction of the nanotube. The reported thermal conductivity values are obtained by averaging over the last 2 ns of the simulations. As quantum effects can play a significant role at temperatures below the Debye temperature of a material,[25] here, we have included the quantum correction of thermal conductivity for nanotubes where the estimated Debye temperature is lower than simulation temperature (300 K). Details of this process can be found in section S1 of the Supporting Information.

$$k_{MD} = -\frac{J}{dT/dZ} \quad (2)$$

3. MD RESULTS

3.1. Thermal Conductivity. To investigate the influence of nanotube length on the thermal conductivity and phonon transport in CNTs and GNTs, nanotubes with lengths ranging from 4 to 200 nm are simulated. The quantum-corrected values of thermal conductivity of CNTs and GNTs are plotted versus nanotube length in Figure 2a,b, respectively. As can be seen in this figure, CNTs possess remarkably higher longitudinal thermal conductivity compared to GNTs at all length scales. Among GNTs, β and γ phases show the lowest and highest thermal conductivities, respectively. It is worthy to note that the higher thermal conductivity of γ-GNT is primarily a result of higher acoustic group velocity and higher volumetric heat capacity because of a denser atomic network. For α- and β-GTNs as well as the CNTs, over most of the nanotube length scales, the thermal conductivity is higher in the armchair form. This is not the case for γ-GNT where the thermal conductivity of armchair and zigzag forms are very similar over the entire range of nanotube lengths.

DOI: 10.1021/acs.jpcc.8b05898
J. Phys. Chem. C 2018, 122, 22688−22698

Equation 3 shows the thermal conductivity as a product of phonon heat capacity, C_{ph} (J m^{-3} K^{-1}), group velocity, u_z (m s^{-1}), relaxation time, τ (s), and MFP, λ (m), integrated over the entire frequency range of each phonon mode. On the basis of eq 3, the thermal conductivity scales linearly with phonon MFP. The length-dependent thermal conductivity at room temperature can be attributed to the variation of phonon MFP.[26,27] In a system with a length scale shorter than the MFP, the heat transfer is dominated by ballistic transport where MFP is limited by scattering at the system boundaries; therefore, the thermal conductivity scales linearly with system length in the ballistic regime. As the system length increases to values larger than the MFP, the phonon transport becomes increasingly more limited by phonon−phonon scattering processes rather than boundary scattering; in this condition, the heat transfer is in the diffusive regime. The rate of phonon−phonon scattering is generally higher for shorter-wavelength phonons.[28] Therefore, in the diffusive transport regime, the contribution of short-wavelength phonons saturates, whereas the contribution of long-wavelength phonons still increases by increasing the system length, leading to an increase in thermal conductivity at a slower pace (i.e., k ≈ L$^{\beta}$, $\beta \leq 0.4$).[29,30]

$$k_{zz} = \int_0^{\nu_{max}} C_{ph} u_z^{\,2} \tau \, d\nu = \int_0^{\nu_{max}} C_{ph} u_z \lambda \, d\nu \quad (3)$$

Figure 3 illustrates the thermal conductivity for all the simulated nanotubes in a log−log plot. It can be seen that the

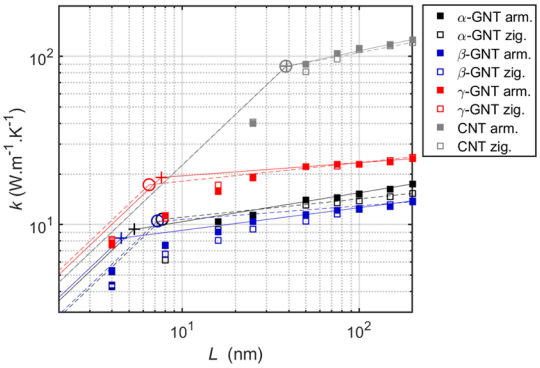

Figure 3. Fitted asymptotic power law curves, $k \propto L^{\beta}$, to different sections of thermal conductivity as a function of length for different nanotubes, shown by a solid line for armchair and a dashed line for zigzag nanotubes. The ballistic to diffusive transition point is shown by cross and ring signs for armchair and zigzag nanotubes, respectively.

thermal conductivities of GNTs and CNTs do not converge at large length scales up to 200 nm and show a power law length dependence. In order to obtain the approximate ballistic to diffusive transition point, two asymptotic power law curves of k $\propto L$ and $k \propto L^{\beta}$ have been fitted to the data at the limits of $L \rightarrow 0$ and $L \rightarrow \infty$, respectively. Refer to section S2 of the Supporting Information for the fitting process. The transition point of a ballistic to a diffusive transport is defined here as the junction of $k \propto L$ and k $\propto L^{\beta}$ curves. The values of transition length and exponent β are listed in Table 1, and in case of CNTs are in agreement with previous studies.[31,32] The transition length of GNTs are within a narrow range of 4.5−7.6 nm, which is significantly shorter compared to the transition length of CNTs. This behavior is due to considerably shorter acoustic phonon MFP of GNTs at room temperature.[33]

Table 1. Ballistic to Diffusive Regime Transition Length and Length Dependence Exponent, β, in the Diffusive Regime ($k \propto L^{\beta}$)

system	ballistic to diffusive transition length (nm)	exponent β in diffusive regime ($k \propto L^{\beta}$)
α-GNT armchair	5.4	0.17
α-GNT zigzag	7.7	0.11
β-GNT armchair	4.5	0.13
β-GNT zigzag	7.2	0.08
γ-GNT armchair	7.6	0.08
γ-GNT zigzag	6.5	0.11
CNT armchair	38.9, comparable to ∼40 nm for (5, 5) CNT in ref 33	0.22, comparable to 0.19 for (5, 5) CNT in ref 33
CNT zigzag	38.5	0.20

In the diffusive region, the length dependence exponent, β, of GNTs falls within a range of 0.08−0.17, which is smaller than the case of CNTs with a value of $\beta \approx 0.2$, consistent with previous studies.[32] This can be attributed to the lower population of long-wavelength phonons in GNTs, showing a weaker contribution to thermal conductivity in the diffusive regime.

4. DISCUSSION

4.1. Phonon Transport. Phonon transport properties of graphyne and CNTs can be identified based on the vibrational phonon density of states [DOS (m^{-3} J^{-1} or m^{-3} erg^{-1})], dispersion relations, and phonon scattering rates. In the MD simulations, the total phonon DOS is calculated by Fourier transformation of the atomic velocity autocorrelation function carried out over all the atoms in the sample as indicated by eq 4.[34]

$$D(\omega) = \int_0^{\infty} e^{-i\omega t} \langle v(t) \cdot v(t) \rangle \, dt \quad (4)$$

Figure 4 depicts the longitudinal phonon DOS for armchair and zigzag orientations of CNTs and GNTs at four different lengths. A significant difference is observed between the DOSs of CNTs and GNTs. CNTs demonstrate a weak peak at ∼22 THz and a stronger peak at around 53 THz, which are attributed to sp^2-bonding networks' bending and stretching modes, respectively.[35−37] The total DOS for GNT samples shows two peaks at around 49 THz and 62−63 THz, which originate from the stretching of C−C and C≡C bonds, respectively. In addition, a peak is observed at 33 THz for α- and β-GNTs, which can be attributed to the interaction or combined stretching of two C−C and one C≡C bonds in series, $\nu_{series} = \left(\frac{1}{\nu_{C-C}^{\,2}} + \frac{1}{\nu_{C\equiv C}^{\,2}} + \frac{1}{\nu_{C-C}^{\,2}} \right)^{-1/2}$, obtaining the value of ∼30 THz, at the edge of the graphyne hexagon. It is also observed that a larger number of high-frequency phonon modes are accessible in GNTs compared to CNTs as the percentage of carbon triple bond increases in the sample, resulting in the dominance of a higher stretching frequency of

DOI: 10.1021/acs.jpcc.8b05898
J. Phys. Chem. C 2018, 122, 22688−22698

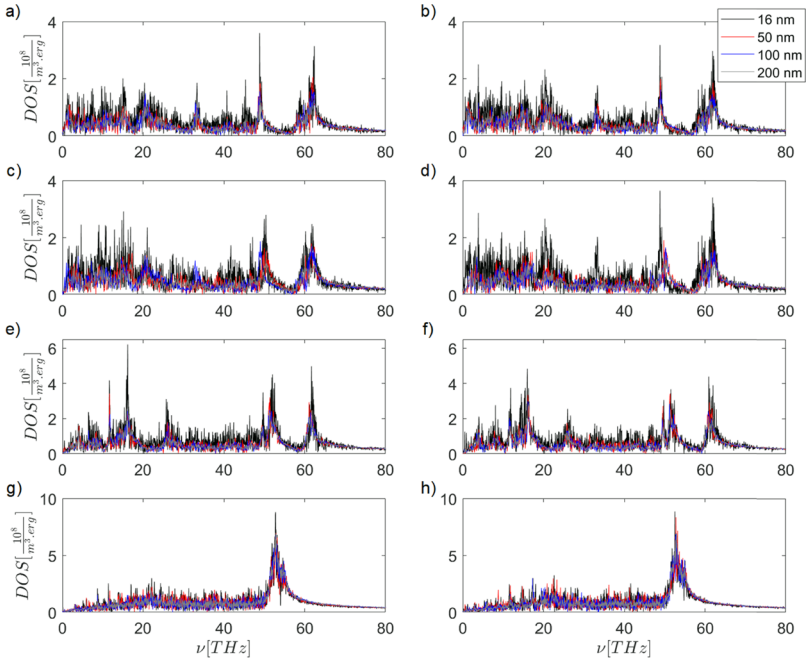

Figure 4. Longitudinal vibrational DOS for (a) armchair α-GNT, (b) zigzag α-GNT, (c) armchair β-GNT, (d) zigzag β-GNT, (e) armchair γ-GNT, (f) zigzag γ-GNT, (g) armchair CNT, and (h) zigzag CNT.

carbon triple bonds. The length dependence of frequency distribution shows a general trend for both GNTs and CNTs in which the population number of high-frequency modes decreases with increasing length as a result of phonon−phonon scattering. On the other hand, the population number of low-frequency modes either slightly increases with increase in length or does not show significant length dependence. Further analysis of the length dependence of DOS can be found in section S3 of the Supporting Information.

In order to obtain important thermal transport parameters such as phonon group velocity and MFP, the dispersion relations are calculated using atomic trajectories extracted from MD simulations. In this analysis, a phonon state is described by wave vector, k, and polarization, p, and has a relaxation time, τ. By transforming the atomic trajectories to the reciprocal space, the time-varying normal mode amplitude $A(k,p,t)$ can be obtained as shown in eq 5.[28]

$$A(k, p, t) = \sum_n (r_n(t) - r_{n_0}) \cdot P_n(k, p) \cdot e^{ik \cdot r_{n_0}} \tag{5}$$

where $r_n(t)$ is the position of the nth atom, r_{n0} is the lattice position, and $P_n(k,p)$ are the corresponding polarization vectors, which are the eigen-vectors of the dynamical matrices obtained from lattice dynamics. For details about calculation of these quantities, refer to ref 28. The phonon dispersion can be obtained by Fourier transformation of the normal mode amplitudes to the frequency domain and capturing the dominant frequency of normal amplitude at each wave vector k and polarization p. Figure 5 illustrates the dispersion curves of CNTs and GNTs in armchair and zigzag orientations; it is noteworthy that the dispersion curves do not show any significant variation with the change in the nanotube length. Four acoustic branches, one longitudinal acoustic (LA), two transverse acoustic (TA), one torsional acoustic (ToA), plus a radial breathing mode, are observed for GNTs and CNTs. The LA and ToA bands demonstrate linear dispersion, whereas the TA band bends slightly for very small k values, which could be consistent with parabolic behavior previously reported for flexural modes of graphene sheet and nanotubes.[38] The acoustic bands in GNTs demonstrate a lower slope at $k = 0$, which leads to lower phonon group velocity of GNTs compared to CNTs.

4.2. Phonon−Phonon Scattering Processes. In the monoatomic lattice of an isolated single-walled CNT or GNT, the phonon relaxation times are primarily controlled by (a) boundary scattering and (b) phonon−phonon scattering processes. For independent scattering processes, the scattering probabilities are additive; hence, the total relaxation time can be obtained by eq 6.

$$\tau^{-1} = \sum_j \tau_j^{-1} \tag{6}$$

The relaxation time because of boundary scattering can be estimated using the relation, $\tau_{b,i} = \frac{FL}{|u_i|}$, where F is a geometric factor which is 1/2 for CNTs;[39] here, we use the same value for GNTs, L is the nanotube lengths, and u_i is the phonon group velocity of mode i. Here, the phonon−phonon interactions are estimated using three-phonon processes where one phonon decays into two other or two phonons combine to form a third phonon. The momentum selection rule and energy conservation for these processes are shown in eqs 7 and 8, respectively, where G is equal to zero in case of a normal (N) process and equal to a reciprocal lattice vector in case of an umklapp process.

$$k \pm k' = k'' + G \tag{7}$$

$$\hbar\omega \pm \hbar\omega' = \hbar\omega'' \tag{8}$$

The relaxation time of the three-phonon umklapp process for a thermal mode k can be obtained using the first-order perturbation theory as shown in eq 9,[40] where γ is the Gruneisen parameter, M is the atomic mass, u_g is the group velocity, n_a is the number of atoms per unit cell, and the Dirac

DOI: 10.1021/acs.jpcc.8b05898
J. Phys. Chem. C 2018, 122, 22688−22698

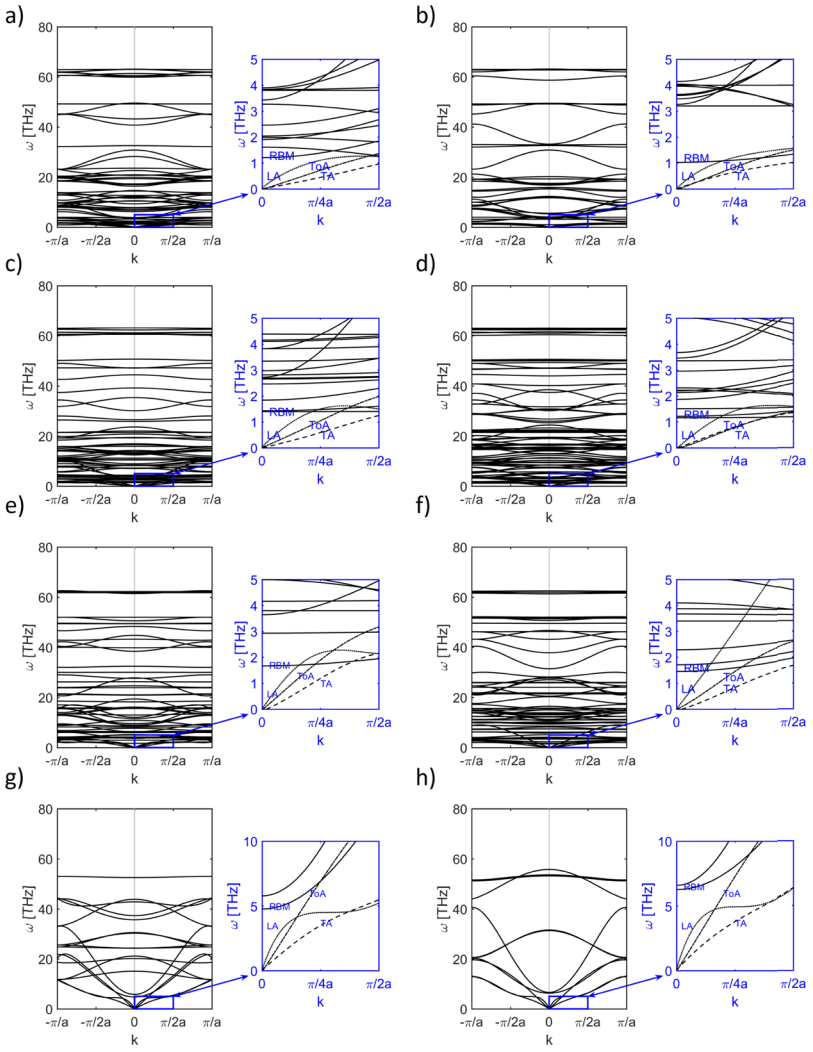

Figure 5. Phonon dispersion relations of (a) armchair α-GNT, (b) zigzag α-GNT, (c) armchair β-GNT, (d) zigzag β-GNT, (e) armchair γ-GNT, (f) zigzag γ-GNT, (g) armchair CNT, and (h) zigzag CNT.

delta function ensures that the energy conservation is satisfied. N_0' and N_0'' are the phonon equilibrium occupancies of modes k' and k'', respectively, given by the Planck distribution. The Gruneisen parameter is shown in eq 10 where u is the acoustic group velocity, C_p is the per mass heat capacity at constant pressure, and α is the linear thermal expansion coefficient. The linear thermal expansion coefficient was obtained for all the nanotubes by varying the MD simulation temperature in the range of 50−400 K in previous studies.[33]

$$\frac{1}{\tau_U} = \sum_{k'} \frac{8\gamma^2 \hbar\omega\omega'\omega''}{3n_a u_g^2 M} \pi\delta(\omega \pm \omega' - \omega'')(N_0' - N_0'') \tag{9}$$

$$\gamma = V\left(\frac{dP}{d\varepsilon}\right)_V = \frac{\alpha u^2}{C_p} \tag{10}$$

In order to obtain the relaxation τ_u at mode k, it is required to integrate over all the possible k' modes using the phonon dispersion relation. The frequencies and wave vectors should satisfy the quasimomentum and energy conservation shown in eqs 7 and 8. In this calculation, all the possible three-phonon scattering events, that are a + a ⇔ a, a + a ⇔ o, a + o ⇔ o, and o + o ⇔ o where o and a stand for optic and acoustic modes, respectively, have been included.

Figure 6 shows the relaxation times in the U-process as a function of wavenumber for different nanotubes and for acoustic and optical modes. It should be noted that, in this figure, the relaxation times shown for optical modes are the average of all optical branches having the same polarization. It can be seen that, for all the nanotubes, the relaxation time of acoustic modes generally increase closer to the k = 0 point. The peaks in the scattering rate appear as local points of low relaxation time in this plot. In addition, it can be seen that the average relaxation times in optic modes are much lower than those of the acoustic modes for all the GNTs; however, that is not the case for CNTs. This indicates that the optical modes in GNTs have on average higher scattering rate, specifically closer to the k = 0 point. Although optical phonons do not directly contribute to thermal conduction, this is an important observation, which can be attributed to the higher energy of optical phonons in GNTs compared to CNTs because of the presence of the acetylene bond.

Furthermore, by statistical analysis of all the phonon−phonon scattering events, the contribution of each of the acoustic and optic modes in the scattering of primary heat transfer modes, that are LA and ToA, can be calculated. To this end, we define P_{YIX} (eq 11) as the probability that in all the U-process events, A + B ⇔ C, phonon B belongs to the mode

DOI: 10.1021/acs.jpcc.8b05898
J. Phys. Chem. C 2018, 122, 22688−22698

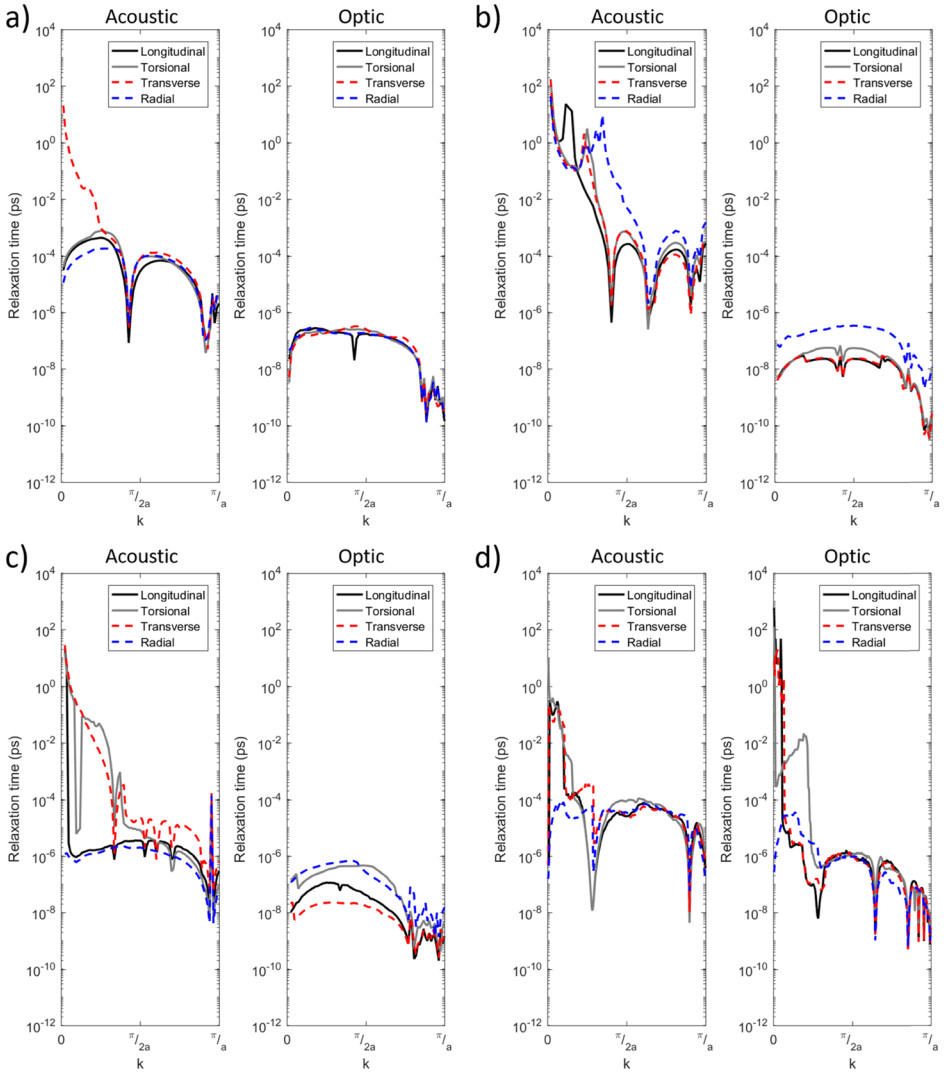

Figure 6. Relaxation times of the U-process as a function of wavenumber for acoustic and optical branches for (a) α-GNT armchair, (b) β-GNT armchair, (c) γ-GNT armchair, and (d) CNT armchair.

Y, given that phonon A belongs to mode X. These probabilities are calculated directly from MD simulations, and the results are shown in Figure 7 for scattering events involving at least one acoustic phonon (i.e., either A or B is an acoustic phonon).

$$\forall\ \mathrm{A, B} \in \{\mathrm{A} + \mathrm{B} \Leftrightarrow \mathrm{C}\};$$
$$P_{\mathrm{Y|X}} = P(\mathrm{B} \in \mathrm{Y|A} \in \mathrm{X}) \tag{11}$$

As can be seen in Figure 7a–c, in all the GNTs, optical phonons have collectively considerably higher contribution to scattering of acoustic phonons in all the polarizations. This is not the case for CNTs, which show a contribution on the same order of magnitude from both acoustic and optical modes in scattering off acoustic modes. Therefore, the primary heat transfer modes in GNTs, LA and ToA bands, are limited by low MFP because of scattering with high-energy optical phonons. This is also reflected in the low length of ballistic to diffusive thermal transport in GNTs.

5. POTENTIAL APPLICATION OF GNTS FOR THERMOELECTRIC ENERGY CONVERSION

Detailed analysis and understanding of the underlying phonon transport mechanism in GNTs enables the use of these materials in energy- and transport-related applications. The authors have previously discussed the application of zigzag α-GNTs as tunable phonovoltaic energy-conversion materials owing to their high occupancy of ultra-high-energy optical phonons (~260 meV), which are more energetic from the direct electronic band gap at room temperature. In this section, we will focus on thermoelectric properties of GNTs as another potential energy-conversion application. The thermoelectric transport properties of γ-GNTs have been previously calculated using density functional-based tight-binding methods for γ-GNTs as a function of tube diameter.[1] However, these calculations have been performed on a supercell containing only a few unit cells. Therefore, the effect of nanotube length and the transition from a ballistic to a diffusive regime has not been studied.

It has been reported by both numerical and experimental studies that the electron MFP in CNTs can be extremely long (10 μm or more); even at room temperature, values higher

DOI: 10.1021/acs.jpcc.8b05898
J. Phys. Chem. C 2018, 122, 22688–22698

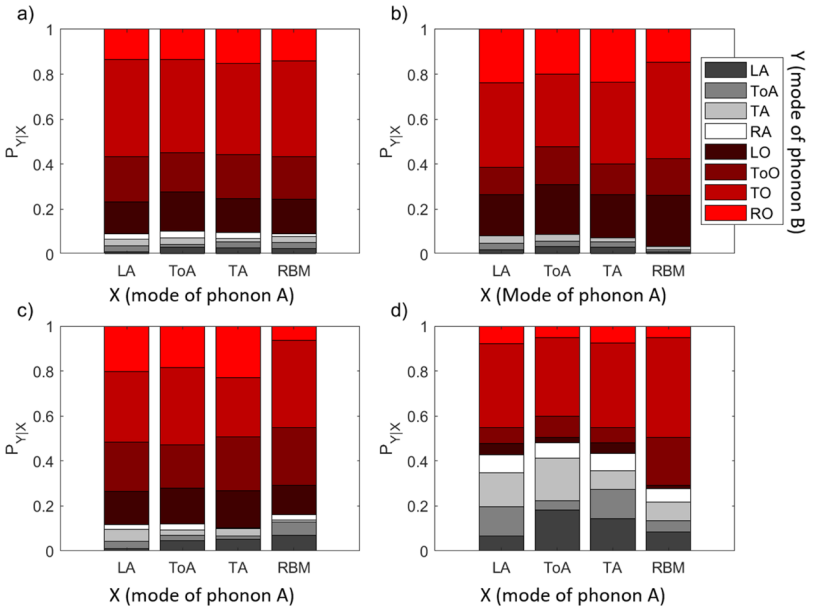

Figure 7. Probability, $P_{Y|X}$, that a phonon, A, with polarization shown in the x-axis, is scattered with a phonon, B, with polarization shown in the figure legend in the U-process: A + B ⇔ C, for (a) α-GNT armchair, (b) β-GNT armchair, (c) γ-GNT armchair, and (d) CNT armchair.

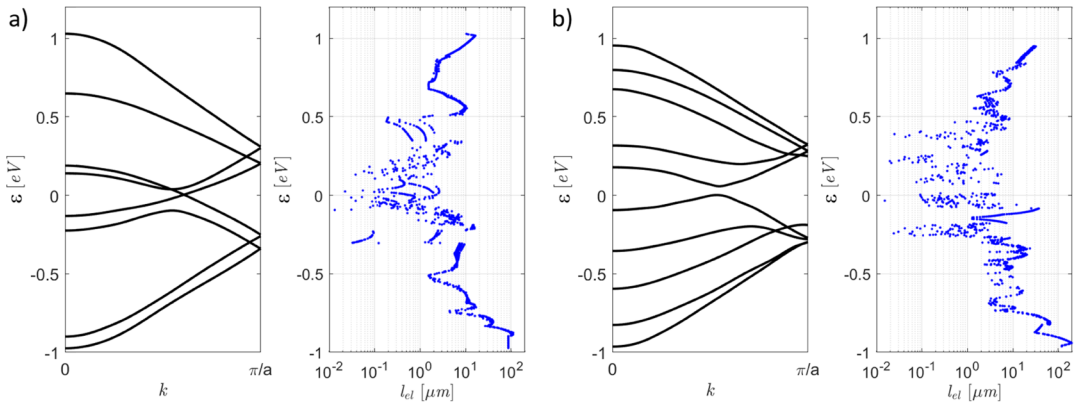

Figure 8. Electronic band structure (from ref 21) and electron MFP obtained from electron−phonon scattering rate estimation (eq 12) for (a) (3, 3) β-GNTs and (b) (4, 4) β-GNTs.

than 1 μm have been reported.[41−43] Here, the electron MFP is estimated using the relation $l_{el} = \tau_{el} v_{g,el}$, where τ_{el} and $v_{g,el}$ are the electron relaxation time and group velocity, respectively. For calculation of the former, we have assumed electron−phonon collision to be the primary mechanism of electron scattering. This assumption is valid here as we are considering a material with no lattice defects where no defect scattering occurs. In addition, unless at very low temperatures, the electron−phonon scattering becomes the dominant mechanism even in the presence of lattice defects. By time-dependent perturbation theory, the total collision rate of an electron at state $|k\rangle$ with phonons at sufficiently high temperatures of $k_B T \gg \hbar v_{ph} k$ can be estimated using eq 12.[44]

$$\frac{1}{\tau_{el}(k)} = \frac{C^2 m^* k k_B T}{\pi v_{ph}{}^2 \rho \hbar^3} \tag{12}$$

In eq 12, the effective mass, $m^* = \frac{\hbar^2}{\partial^2 \varepsilon / \partial k^2}$ (kg), and the electron group velocity, $v_{el} = \frac{1}{\hbar}\frac{\partial \varepsilon}{\partial k}$, have been calculated from the electronic band structures of GNTs obtained from ref 21.

Figure 8 shows the electronic band structure[21] as well as the wave vector-averaged electron MFP as a function of energy for (3, 3) and (4, 4) β-GNTs as two examples. It can be seen that the electron MFP can be extremely long, of order 1 μm and above, for a large range of electron energies. This calculation is consistent with previous theoretical studies on electronic transport in a graphyne sheet, which have suggested higher electron mobility and therefore MFP for graphynes compared to graphene because of a lower rate of electron−phonon scattering.[45]

Therefore, in GNTs, the ballistic to diffusive transition length is ultralow for phonons, less than 10 nm, whereas it is extremely long for electrons, on average ∼1 μm for armchair β-GNTs. This behavior potentially can lead to a high thermoelectric figure of merit in long GNTs as discussed below. Equation 13 shows the thermoelectric figure of merit, ZT, where G, C, and S are the electrical conductance, thermal conductance, and Seebeck coefficient, respectively.[46]

$$ZT = \frac{G S^2 T}{C} \tag{13}$$

DOI: 10.1021/acs.jpcc.8b05898
J. Phys. Chem. C 2018, 122, 22688−22698

Figure 9 shows the calculated values of electrical conductance based on the relaxation time approximation and

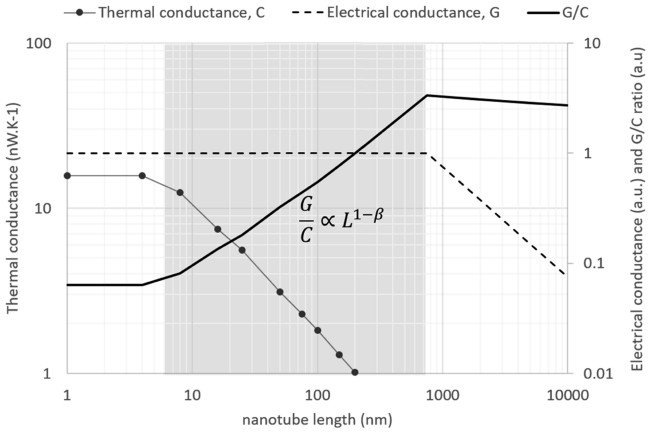

Figure 9. Thermal and electrical transport regimes of (3, 3) β-GNT at 300 K. The central grayed region indicates diffusive thermal and ballistic electrical transport where G/C ratio is expected to increase with nanotube length. The thermal conductance shows a calculated value based on MD simulations; however, the electrical conductance shows the estimated trend.

thermal conductance based on the NEMD calculations as a function of nanotube length for (4, 4) β-GNT. It can be seen that the electronic transport remains ballistic for a large range of nanotube lengths; therefore, for a ballistic channel, the conductance remains constant (equal to quantum conductance G_0) as the nanotube length increases. However, the phonon transport becomes diffusive in much shorter length scales, leading to reduction in thermal conductance as a function of nanotube length. This behavior can lead to improved ZT as the nanotube length increases in a wide range of length scales where the thermal transport is diffusive and electronic transport is ballistic. The dependence of ZT on nanotube length has a functional form of $ZT \propto S(L)^2 L^{(1-\beta)}$, where β is the power law exponent of thermal conductivity in the diffusive regime, which is ~0.1 for the β-GNT in Figure 9.[46] Therefore, compared to the first principle calculations in the purely ballistic regime, it is expected that the ZT value would enhance as the nanotube length increases up to an extremely long length of order micrometer. The theoretical discussion in this section and the expected trends of ZT are of a qualitative nature. The quantitative calculation of ZT as a function of length for long GNTs can be done within the relaxation time approximation of the Boltzmann transport equation,[46,47] which is the subject of future research.

6. CONCLUSIONS

The phonon transport properties of α-, β-, and γ-GNTs as well as a CNTs with armchair and zigzag orientations in thermal transport regimes ranging from ballistic to diffusive are studied using NEMD by varying the nanotube length from 4 to 200 nm at room temperature. It was observed that the thermal conductivity is noticeably higher for CNTs compared to different types of GNTs across the entire ballistic−diffusive region. This is due to significantly lower acoustic group velocity, shorter phonon relaxation times, and lower atomic network density of GNTs compared to CNTs. Furthermore, among all simulated GNTs, γ and β phases seemed to have the lowest and highest thermal conductivities, respectively. Similarly, the cause of the difference in thermal conductivity among GNTs is mainly the difference in acoustic group velocity and atomic network density.

The thermal conductivity does not converge at lengths up to 200 nm for both GNTs and CNTs. A quantitative value of the ballistic to diffusive transition length is obtained as the junction of $k \propto L$ and $k \propto L^{\beta}$ asymptotes of the thermal conductivity versus nanotube length curve. The rate of increase in thermal conductivity as a function of length in the diffusive regime, that is β, is smaller in GNTs compared to CNTs. It is observed that the transition lengths of all the GNT structures studied here fall within a range of 4.5−7.3 nm at room temperature, which is significantly shorter than that of CNTs with a transition length of ~39 nm. Ultralow acoustic phonon MFP is the primary contributor to this behavior, which is caused by a lower acoustic phonon group velocity and significantly shorter acoustic phonon relaxation times in GNTs compared to CNTs.

To gain a mechanistic insight into the scattering process, the rate of phonon−phonon scattering is estimated by three-phonon processes. A statistical analysis of the umklapp scattering events indicates that in the GNT lattice, irrespective of the phonon polarization, it is highly probable that the acoustic phonons which are the main heat carriers be scattered off a highly energetic optical phonon which is generated by acetylene bonds in GNTs. Conversely, in CNTs, both optical and acoustic phonons have similar contributions to scattering heat carriers. Although the high-energy optical modes in GNTs do not directly contribute to heat conduction, they play a major role in inhibiting thermal transport by limiting the MFP of primary conduction bands, LA and ToA, which is in accordance with the small ballistic to diffusive transition length of thermal transport in GNTs. The ultralow phonon MFP, as well as extremely large micrometer-scale electron MFP at room temperature in GNTs, provides a pathway toward obtaining a high thermoelectric figure of merit in long GNTs.

■ ASSOCIATED CONTENT

Supporting Information

The Supporting Information is available free of charge on the ACS Publications website at DOI: 10.1021/acs.jpcc.8b05898.

Calculation of quantum correction of thermal conductivity values; method for calculation of transition length of ballistic to diffusive transport regimes; and length dependence of phonon DOS in nanotubes (PDF)

■ AUTHOR INFORMATION

Corresponding Author

*E-mail: ramazani@mit.edu.

ORCID

Ali Ramazani: 0000-0002-6887-1086

Author Contributions

#A.R. and A.S. have equal contribution.

Notes

The authors declare no competing financial interest.

■ ACKNOWLEDGMENTS

The authors would like to acknowledge the use of University of Michigan's Advanced Research Computing Cluster for carrying out the simulations.

DOI: 10.1021/acs.jpcc.8b05898
J. Phys. Chem. C 2018, 122, 22688−22698

REFERENCES

(1) Wang, X.-M.; Lu, S.-S. Thermoelectric Transport in Graphyne Nanotubes. *J. Phys. Chem. C* **2013**, *117*, 19740−19745.
(2) Lukes, J. R.; Zhong, H. Thermal Conductivity of Individual Single-Wall Carbon Nanotubes. *J. Heat Transfer* **2007**, *129*, 705−716.
(3) Pereira, L. F. C.; Savić, I.; Donadio, D. Thermal Conductivity of One-, Two- and Three-Dimensional Sp 2 Carbon. *New J. Phys.* **2013**, *15*, 105019.
(4) Ren, C.; Zhang, W.; Xu, Z.; Zhu, Z.; Huai, P. Thermal Conductivity of Single-Walled Carbon Nanotubes under Axial Stress. *J. Phys. Chem. C* **2010**, *114*, 5786−5791.
(5) Zhang, Y. Y.; Pei, Q. X.; Wang, C. M. A Molecular Dynamics Investigation on Thermal Conductivity of Graphynes. *Comput. Mater. Sci.* **2012**, *65*, 406−410.
(6) Kim, P.; Shi, L.; Majumdar, A.; McEuen, P. L. Thermal Transport Measurements of Individual Multiwalled Nanotubes. *Phys. Rev. Lett.* **2001**, *87*, 215502.
(7) Guthy, C.; Du, F.; Brand, S.; Winey, K. I.; Fischer, J. E. Thermal Conductivity of Single-Walled Carbon Nanotube/PMMA Nanocomposites. *J. Heat Transfer* **2007**, *129*, 1096−1099.
(8) Wang, Z.; Tang, D.; Zheng, X.; Zhang, W.; Zhu, Y. Length-Dependent Thermal Conductivity of Single-Wall Carbon Nanotubes: Prediction and Measurements. *Nanotechnology* **2007**, *18*, 475714.
(9) Zhong, H.; Lukes, J. R. Interfacial Thermal Resistance between Carbon Nanotubes: Molecular Dynamics Simulations and Analytical Thermal Modeling. *Phys. Rev. B: Condens. Matter Mater. Phys.* **2006**, *74*, 125403.
(10) Volz, S. G.; Chen, G. Molecular Dynamics Simulation of Thermal Conductivity of Silicon Nanowires. *Appl. Phys. Lett.* **1999**, *75*, 2056−2058.
(11) Wang, S.-c.; Liang, X.-g.; Xu, X.-h.; Ohara, T. Thermal Conductivity of Silicon Nanowire by Nonequilibrium Molecular Dynamics Simulations. *J. Appl. Phys.* **2009**, *105*, 014316.
(12) Evans, D. J. Homogeneous NEMD algorithm for thermal conductivity-Application of non-canonical linear response theory. *Phys. Lett. A* **1982**, *91*, 457−460.
(13) Salaway, R. N.; Zhigilei, L. V. Molecular Dynamics Simulations of Thermal Conductivity of Carbon Nanotubes: Resolving the Effects of Computational Parameters. *Int. J. Heat Mass Transfer* **2014**, *70*, 954−964.
(14) Alaghemandi, M.; Algaer, E.; Böhm, M. C.; Müller-Plathe, F. The Thermal Conductivity and Thermal Rectification of Carbon Nanotubes Studied Using Reverse Non-Equilibrium Molecular Dynamics Simulations. *Nanotechnology* **2009**, *20*, 115704.
(15) Cranford, S. W.; Buehler, M. J. Mechanical Properties of Graphyne. *Carbon* **2011**, *49*, 4111−4121.
(16) Coluci, V. R.; Braga, S. F.; Legoas, S. B.; Galvão, D. S.; Baughman, R. H. Families of Carbon Nanotubes: Graphyne-Based Nanotubes. *Phys. Rev. B: Condens. Matter Mater. Phys.* **2003**, *68*, 035430.
(17) Wang, J.; Zhang, A.-J.; Tang, Y. Tunable Thermal Conductivity in Carbon Allotrope Sheets: Role of Acetylenic Linkages. *J. Appl. Phys.* **2015**, *118*, 195102.
(18) Pan, C.-N.; Chen, X.-K.; Tang, L.-M.; Chen, K.-Q. Orientation Dependent Thermal Conductivity in Graphyne Nanoribbons. *Phys. E* **2014**, *64*, 129−133.
(19) Hu, M.; Jing, Y.; Zhang, X. Low Thermal Conductivity of Graphyne Nanotubes from Molecular Dynamics Study. *Phys. Rev. B: Condens. Matter Mater. Phys.* **2015**, *91*, 155408.
(20) Plimpton, S. Fast Parallel Algorithms for Short-Range Molecular Dynamics. *J. Comput. Phys.* **1995**, *117*, 1−19.
(21) Cao, A.; Qu, J. Size Dependent Thermal Conductivity of Single-Walled Carbon Nanotubes. *J. Appl. Phys.* **2012**, *112*, 013503.
(22) Hoover, W. G. Canonical Dynamics: Equilibrium Phase-Space Distributions. *Phys. Rev. A: At., Mol., Opt. Phys.* **1985**, *31*, 1695−1697.
(23) Soleimani, A.; Araghi, H.; Zabihi, Z.; Alibakhshi, A. A Comparative Study of Molecular Dynamics Simulation Methods for Evaluation of the Thermal Conductivity and Phonon Transport in Si Nanowires. *Comput. Mater. Sci.* **2018**, *142*, 346−354.
(24) Yang, Y. W.; Liu, X. J.; Yang, J. P. Nonequilibrium Molecular Dynamics Simulation for Size Effects on Thermal Conductivity of Si Nanostructures. *Mol. Simul.* **2008**, *34*, 51−56.
(25) Turney, J. E.; McGaughey, A. J. H.; Amon, C. H. Assessing the Applicability of Quantum Corrections to Classical Thermal Conductivity Predictions. *Phys. Rev. B: Condens. Matter Mater. Phys.* **2009**, *79*, 224305.
(26) Wang, Z. L.; Tang, D. W.; Li, X. B.; Zheng, X. H.; Zhang, W. G.; Zheng, L. X.; Zhu, Y. T.; Jin, A. Z.; Yang, H. F.; Gu, C. Z. Length-Dependent Thermal Conductivity of an Individual Single-Wall Carbon Nanotube. *Appl. Phys. Lett.* **2007**, *91*, 123119.
(27) Zhang, G.; Li, B. Thermal Conductivity of Nanotubes Revisited: Effects of Chirality, Isotope Impurity, Tube Length, and Temperature. *J. Chem. Phys.* **2005**, *123*, 114714.
(28) Henry, A. S.; Chen, G. Spectral Phonon Transport Properties of Silicon Based on Molecular Dynamics Simulations and Lattice Dynamics. *J. Comput. Theor. Nanosci.* **2008**, *5*, 141−152.
(29) Kaburaki, H.; Machida, M. Thermal Conductivity in One-Dimensional Lattices of Fermi-Pasta-Ulam Type. *Phys. Lett. A* **1993**, *181*, 85−90.
(30) Wang, J.-S.; Li, B. Intriguing Heat Conduction of a Chain with Transverse Motions. *Phys. Rev. Lett.* **2004**, *92*, 074302.
(31) Wang, J.; Wang, J.-S. Carbon Nanotube Thermal Transport: Ballistic to Diffusive. *Appl. Phys. Lett.* **2006**, *88*, 111909.
(32) Shiomi, J.; Maruyama, S. Molecular Dynamics of Diffusive-Ballistic Heat Conduction in Single-Walled Carbon Nanotubes. *Jpn. J. Appl. Phys.* **2008**, *47*, 2005.
(33) Ramazani, A.; Reihani, A.; Soleimani, A.; Larson, R.; Sundararaghavan, V. Molecular Dynamics Study of Phonon Transport in Graphyne Nanotubes. *Carbon* **2017**, *123*, 635−644.
(34) Kong, L. T. Phonon Dispersion Measured Directly from Molecular Dynamics Simulations. *Comput. Phys. Commun.* **2011**, *182*, 2201−2207.
(35) Dresselhaus, M. S.; Jorio, A.; Hofmann, M.; Dresselhaus, G.; Saito, R. Perspectives on Carbon Nanotubes and Graphene Raman Spectroscopy. *Nano Lett.* **2010**, *10*, 751−758.
(36) Kim, U. J.; Furtado, C. A.; Liu, X.; Chen, G.; Eklund, P. C. Raman and IR Spectroscopy of Chemically Processed Single-Walled Carbon Nanotubes. *J. Am. Chem. Soc.* **2005**, *127*, 15437−15445.
(37) Mohan, J. *Organic Spectroscopy: Principles and Applications*; Crc Press, 2004.
(38) Jiang, J.-W.; Wang, B.-S.; Wang, J.-S.; Park, H. S. A Review on the Flexural Mode of Graphene: Lattice Dynamics, Thermal Conduction, Thermal Expansion, Elasticity and Nanomechanical Resonance. *J. Phys.: Condens. Matter* **2015**, *27*, 083001.
(39) Lindsay, L.; Broido, D. A.; Mingo, N. Lattice Thermal Conductivity of Single-Walled Carbon Nanotubes: Beyond the Relaxation Time Approximation and Phonon-Phonon Scattering Selection Rules. *Phys. Rev. B: Condens. Matter Mater. Phys.* **2009**, *80*, 125407.
(40) Cao, J. X.; Yan, X. H.; Xiao, Y.; Ding, J. W. Thermal Conductivity of Zigzag Single-Walled Carbon Nanotubes: Role of the Umklapp Process. *Phys. Rev. B: Condens. Matter Mater. Phys.* **2004**, *69*, 073407.
(41) White, C. T.; Todorov, T. N. Carbon Nanotubes as Long Ballistic Conductors. *Nature* **1998**, *393*, 240−242.
(42) Purewal, M. S.; Hong, B. H.; Ravi, A.; Chandra, B.; Hone, J.; Kim, P. Scaling of Resistance and Electron Mean Free Path of Single-Walled Carbon Nanotubes. *Phys. Rev. Lett.* **2007**, *98*, 186808.
(43) Li, H. J.; Lu, W. G.; Li, J. J.; Bai, X. D.; Gu, C. Z. Multichannel Ballistic Transport in Multiwall Carbon Nanotubes. *Phys. Rev. Lett.* **2005**, *95*, 086601.
(44) Kittel, C.; Fan, H. Y. Introduction to Solid State Physics. *Am. J. Phys.* **1957**, *25*, 330.
(45) Chen, J.; Xi, J.; Wang, D.; Shuai, Z. Carrier Mobility in Graphyne Should Be Even Larger than That in Graphene: A Theoretical Prediction. *J. Phys. Chem. Lett.* **2013**, *4*, 1443−1448.
(46) Scheidemantel, T. J.; Ambrosch-Draxl, C.; Thonhauser, T.; Badding, J. V.; Sofo, J. O. Transport Coefficients from First-Principles

DOI: 10.1021/acs.jpcc.8b05898
J. Phys. Chem. C 2018, 122, 22688−22698

Calculations. *Phys. Rev. B: Condens. Matter Mater. Phys.* **2003**, *68*, 125210.
(47) Bulusu, A.; Walker, D. G. Review of Electronic Transport Models for Thermoelectric Materials. *Superlattices Microstruct.* **2008**, *44*, 1−36.

DOI: 10.1021/acs.jpcc.8b05898
J. Phys. Chem. C 2018, 122, 22688−22698